New Phytologist

Research

Quantifying vulnerability to embolism in tropical trees and lianas using five methods: can discrepancies be explained by xylem structural traits?

Ya-Jun Chen[1,2,3]*, Phisamai Maenpuen[1,4]*, Yong-Jiang Zhang[5], Kallol Barai[5], Masatoshi Katabuchi[1,2], Hui Gao[1,4], Sasiwimol Kaewkamol[1,4], Lian-Bin Tao[1] and Jiao-Lin Zhang[1,2]

[1]CAS Key Laboratory of Tropical Forest Ecology, Xishuangbanna Tropical Botanical Garden, Chinese Academy of Sciences, Mengla, Yunnan 666303, China; [2]Center of Plant Ecology, Core Botanical Gardens, Chinese Academy of Sciences, Mengla, Yunnan 666303, China; [3]Yuanjiang Savanna Ecosystem Research Station, Xishuangbanna Tropical Botanical Garden, Chinese Academy of Sciences, Yuanjiang, Yunnan 653300, China; [4]University of Chinese Academy of Sciences, Beijing 100049, China; [5]School of Biology and Ecology, University of Maine, Orono, ME 04469, USA

Authors for correspondence:
Ya-Jun Chen
Email: chenyj@xtbg.org.cn

Yong-Jiang Zhang
Email: yongjiang.zhang@maine.edu

Jiao-Lin Zhang
Email: zjl@xtbg.org.cn

Received: *23 March 2020*
Accepted: *18 August 2020*

New Phytologist (2021) **229:** 805–819
doi: 10.1111/nph.16927

Key words: cavitation resistance, drought tolerance, embolism, hydraulic architecture, lianas, tree mortality, X-ray MicroCT.

Summary

- Vulnerability curves (VCs) describe the loss of hydraulic conductance against increasing xylem tension, providing valuable insights about the response of plant water transport to water stress. Techniques to construct VCs have been developed and modified continuously, but controversies continue.
- We compared VCs constructed using the bench-top dehydration (BD), air-injection-flow (AI), pneumatic-air-discharge (PAD), optical (OP) and X-ray-computed microtomography (MicroCT) methods for tropical trees and lianas with contrasting vessel lengths.
- The PAD method generated highly vulnerable VCs, the AI method intermediate VCs, whereas the BD, OP and MicroCT methods produced comparable and more resistant VCs. Vessel-length and diameter accounted for the overestimation ratio of vulnerability estimated using the AI but not the PAD method. Compared with directly measured midday embolism levels, the PAD and AI methods substantially overestimated embolism, whereas the BD, MicroCT and OP methods provided more reasonable estimations.
- Cut-open vessels, uncertainties in maximum air volume estimations, sample-length effects, tissue cracks and shrinkage together may impede the reliability of the PAD method. In conclusion, we validate the BD, OP and MicroCT methods for tropical plants, whereas the PAD and AI need further mechanistic testing. Therefore, applications of VCs in estimating plant responses to drought need to be cautious.

Introduction

The long-distance water transport of plants is under negative pressure, as explained by the Cohesion-Tension theory (Dixon & Joly, 1895; Tyree & Zimmermann, 2002). This metastable state leads to a risk of cavitation (i.e. the appearance of a vapor phase within the liquid phase), which occurs when water undergoes an abrupt phase change from liquid to gas or air bubbles are pulled into the conduits through bordered pits (air seeding). The phenomenon that a xylem conduit becomes gas-filled (embolized), obstructing the long-distance water transport, is termed embolism (Zimmermann, 1983). Xylem dysfunction caused by embolism is considered one of the main processes that occurs under severe drought conditions which can result in a series of problems and ultimately mortality of plants (McDowell *et al.*, 2008; McDowell, 2011; Anderegg *et al.*, 2012, 2016; Choat *et al.*, 2018). Xylem embolism resistance is one of the most important traits determining plant drought resistance, and a significant factor in explaining massive drought-induced plant deaths in recent years (Allen *et al.*, 2010; Choat *et al.*, 2012, 2018) and predicting forest response to future climate change scenarios (Reichstein *et al.*, 2013). An understanding of xylem embolism resistance is one of the central interests in plant physiology and ecology.

Xylem resistance to embolism is often determined by vulnerability curves (VCs) which describe how the percentage loss of hydraulic conductance (PLC) or xylem embolism increases when xylem water potential decreases (xylem tension increases). Vulnerability curves can provide valuable information about the drought responses of particular plants and have been used to quantify plant drought resistance and ecological adaptations (Tyree & Ewers, 1991). For example, xylem tensions at 50% (or 88%) loss of hydraulic conductivity (P_{50} or P_{88}), and hydraulic

*These authors contributed equally to this work.

safety margins (the difference between minimum xylem water potential and P_{50}) are widely used to quantify drought resistance and the risk of hydraulic impairment (Choat *et al.*, 2012; Skelton *et al.*, 2015; Anderegg *et al.*, 2016, 2018).

In the past decades, significant efforts have been made to develop reliable techniques to accurately detect and quantify xylem embolism (reviewed by Cochard *et al.*, 2013). Since the first VC was published, a growing number of techniques have been developed to construct VCs for different plant organs and, consequently, a large number of VCs already have been produced (Sperry *et al.*, 1988; Choat *et al.*, 2012; Cochard *et al.*, 2013; Cai *et al.*, 2014). The VC techniques differ mainly in how xylem embolism is induced or detected. Embolism induction techniques include the bench-top dehydration method (Sperry *et al.*, 1988), the air-injection-flow method (Sperry & Tyree, 1990; Cochard *et al.*, 1992), and the static- (Alder *et al.*, 1997) or flow-centrifuge (i.e. Cavitron) method (Cochard *et al.*, 2005). Both the air-injection-flow and the centrifuge methods enable manual control of the applied pressure (or xylem tension) with good accuracy and lower sample and time consumption compared to the bench-top dehydration method. However, they are both prone to artifacts (Cochard *et al.*, 2013; Wang *et al.*, 2014; Zhang & Holbrook, 2014). Embolism detection techniques include the widely used hydraulic measurement method (i.e. measure water flow through a stem segment using the apparatus by Sperry *et al.*, (1988) to estimate embolism level, hereafter 'hydraulic method'), the acoustic detection method (Milburn & Johnson, 1966), the pneumatic-air-discharge method (Pereira *et al.*, 2016, 2020), the optical method (Brodribb *et al.*, 2016a, 2017) and the X-ray imaging method (Brodersen *et al.*, 2010). Despite having potential artifacts (Skelton & Diaz, 2020), the bench-top dehydration method (measured hydraulically) often is used as a reference method to validate other methods. The X-ray imaging method includes synchrotron-based or benchtop-based X-ray computed tomography (CT). The synchrotron-based CT uses a much greater flux of X-rays with a parallel beam which allows scanning of large samples in a shorter time compared to the benchtop-based system which is restricted mostly to excised, relatively small samples. Both the X-ray imaging and optical methods enable researchers to visualize the process of embolism occurrence and spread. Using a principally different approach, the pneumatic-air-discharge (PAD) method (or its new version, Pneumatron) quantifies xylem embolism based on gas diffusion from embolized vessels and is a nonhydraulic, low-cost method with high temporal resolution. The PAD method generated P_{50} values comparable to other methods (e.g. bench-top dehydration, air-injection-flow and flow-centrifuge methods) in 18 angiosperms species, whereas two ring-porous angiosperm and two gymnosperm species showed great differences between the PAD and reference methods (Pereira *et al.*, 2016, 2020; Zhang *et al.*, 2018).

Although methods for constructing VCs have been continuously developed or modified, the controversy about the reliability of different methods is ongoing (Choat *et al.*, 2010; Cochard *et al.*, 2013; Cai *et al.*, 2014; Rockwell *et al.*, 2014; Jansen *et al.*, 2015; Venturas *et al.*, 2017, 2019; Pratt *et al.*, 2020). One such example is the VCs for grapevine, which has been intensively studied for many decades, where no agreement has yet been reached because different methods usually generate contrasting results (Cochard *et al.*, 2010; Gambetta *et al.*, 2020). Another example is the widely studied species *Laurus nobilis* which also is prone to methodological artifacts, leading to largely inconsistent views regarding its vulnerability to embolism among studies (Charrier *et al.*, 2016). Even the bench-top dehydration method, the conventional 'gold reference', has often been challenged because of artifacts during the sample preparation and measurements (Cochard *et al.*, 2013; Sperry, 2013; Wheeler *et al.*, 2013; Torres-Ruiz *et al.*, 2015; Skelton & Diaz, 2020). As a consequence of artifacts during sample preparation and/or measurement processes, many techniques are argued to be species-dependent (Cochard *et al.*, 2013; Venturas *et al.*, 2017). In the past decade, at least 19 studies have evaluated the reliability of the different methods (Supporting Information Table S1); however, compared to temperate species, species from tropical wet forests with typically long vessels (Gao *et al.*, 2019) are relatively less studied. Moreover, studies testing different methods using multiple species with a large range of conduit size are relatively rare.

In this study, we first determined the VCs for five tropical woody species with contrasting vessel lengths using five techniques, including two widely used methods: the bench-top dehydration and the air-injection-flow methods, as well as the recently developed PAD, optical and X-ray imaging methods. Because most species from tropical wet forests have long vessels (Ewers & Fisher, 1987; Jacobsen *et al.*, 2012), we excluded the centrifuge method from our comparison as it appears to be suitable only for short-vessel species (Cochard *et al.*, 2013). Secondly, we determined the native embolism in the field and compared this to predicted values derived from the VCs constructed by different techniques and xylem tensions. Additionally, we also tested whether the discrepancies in results from different methods were species-dependent and could be explained by the differences in xylem structural traits. The main objectives of this study were to: (1) quantify the variances in VCs generated using different techniques for identical plant materials, (2) reveal the underlying artifacts or biases in some techniques when applied to long-vessel tropical plants, and (3) explore whether the application of some techniques is species-dependent, and can be explained by differences in xylem anatomy.

Materials and Methods

Site and species information

We conducted this study in a tropical limestone forest nearby Xishuangbanna Tropical Botanical Garden, Chinese Academy of Sciences (XTBG, lat. 21°41′N, long. 101°25′E, 570 m asl), Yunnan, Southwest China. This region has a typical tropical monsoon climate. The mean annual precipitation is approximately 1560 mm, and the mean annual temperature is 21.7°C (Cao *et al.*, 2006). Most precipitation (*c.* 80%) occurs in the wet season (May to October). There is a distinct dry period from November to April.

Based on our previous work (Gao *et al.*, 2019), five common species (three trees and two lianas) were chosen for this study to cover a range of relatively short- to long-vessel species. The maximum vessel lengths (MVL, cm) were determined before all measurements (see Methods S1). The five species differed in maximum vessel length (Table 1) as follows – short-vessel species (< 50 cm): *Microcos paniculate* and *Lasiococca comberi* (trees); medium-vessel species (50–100 cm): *Lagerstroemia tomentosa* (trees); and long-vessel species (> 100 cm): *Combretum yunnanense* and *Combretum griffithii* (lianas). We tagged 20–30 mature, healthy, similar-sized individuals of each species in the field and randomly harvested sun-exposed branch samples were from these tagged individuals.

Vulnerability curve determinations using different methods

We used the bench-top dehydration technique (measured hydraulically, likewise hereinafter; Sperry *et al.*, 1988; Torres-Ruiz *et al.*, 2015), the optical method (Brodribb *et al.*, 2016b), the air-injection-flow method (Cochard *et al.*, 1992), the pneumatic-air-discharge method (Pereira *et al.*, 2016) and the X-ray-computed microtomography (MicroCT) imaging method (Cochard *et al.*, 2015; Choat *et al.*, 2016) to construct vulnerability curves (VCs) for all five species during the 2019 wet season.

We collected all samples before sunrise (between 06:00 h and 07:00 h solar time). Tree and liana branch samples for VC measurements were cut as long as possible (2–2.5 m and 4–5 m, respectively). The excised branches were cut underwater *c.* 20 cm from the basal ends (not necessary for VC determinations) and then the cut ends of all excised branches were wrapped with wet paper towels (notably, a better approach is keeping branches underwater if feasible). The whole branches were sprayed with water, placed in large black plastic bags to prevent water loss, and transported to the laboratory within 1 h.

The bench-top dehydration (BD) method In order to construct BD-VCs, we used 20–30 large leafy branches (harvested as described above) from ≥ 10 tagged individuals of each species. Under laboratory room conditions, all branches were dehydrated to different dehydration conditions. Leaves from each branch were sampled periodically to determine water potential (Ψ_{leaf}, MPa) using a pressure chamber (PMS1505D-EXP, PMS Instrument Company, Corvallis, OR, USA). Once a targeted dehydration condition was reached, branches were bagged with water vapor saturated bags for ≥ 1 h to reach homogeneity in water potential along the entire branch. Afterwards, two bagged leaves (or terminal twigs) from different positions along each branch were cut to test equilibrium in Ψ_{leaf}. We used the average of the two Ψ_{leaf} measurements to represent xylem tension when the difference between them was < 0.3 MPa. To avoid 'cutting under tension' artifacts (Wheeler *et al.*, 2013; Torres-Ruiz *et al.*, 2015), the branches with all leaves bagged were cut underwater 30 cm from the basal ends to release tension until Ψ_{leaf} was close to zero. We cut two adjacent 10-cm-long segments (5–8 mm in diameter) underwater at postions ~ 20 cm to 50 cm apart from the apex, depending on the species. The two segments were used for hydraulic measurements and MicroCT scans, respectively. In the case of large samples with multibranching, we cut an additional pair of 10-cm-long segments from a side branch to represent within-branch variance.

Using a sharp blade, one 10-cm-long segment was trimmed at both ends then connected to a hydraulic measurement system with a 1 kPa (10 cm hydrostatic pressure) and 10 mM degassed and filtered (0.2 μm) KCl solution. The distal end of the segment was connected to a pipette, then an initial conductance (K_0) of the segment was determined as:

$$K = F/P \quad \text{Eqn 1}$$

(F and P, water flux and hydrostatic pressure, respectively).

The maximum conductance (K_{max}) was determined again after flushing the segment with 100 kPa pressure KCl solution for over 1 h. The percentage loss of hydraulic conductance (PLC) was calculated as:

$$PLC = 100 \times (K_{max} - K_0)/K_{max} \quad \text{Eqn 2}$$

Finally, 40–50 PLC values from 20–30 branches were obtained for each species to construct VCs.

The air-injection-flow (AI) method Although the AI method has been challenged (Ennajeh *et al.*, 2011; Cochard *et al.*, 2013; Yin & Cai, 2018), it is still used by researchers and we included it here to test if the reliability depends on xylem structural traits. We used a commercial double-ended pressure sleeve (PMS1505D-EXP, PMS Instrument Company) in this study. The chamber was 2.5 cm in diameter and 8 cm in length. Six to ten branches from at least six individuals per species were used to

Table 1 Species information for this study.

Species	Family	Phenology	Lifeform	MVL (cm)	D_h (μm)
Microcos paniculate L.	Malvaceae	E	Tree	37.3 ± 2.6	60.69 ± 3.0
Lasiococca comberi Haines	Euphorbiaceae	E	Tree	39.3 ± 1.6	53.73 ± 1.8
Lagerstroemia tomentosa C. Presl	Lythraceae	D	Tree	99.8 ± 10.6	76.04 ± 5.3
Combretum yunnanense Exell	Combretaceae	D	Liana	126.5 ± 8.3	87.82 ± 2.36
Combretum griffithii Van Heurck & Müll. Arg.	Combretaceae	D	Liana	141.0 ± 15.2	108.92 ± 10.0

E, evergreen; D, deciduous; MVL, maximum vessel length; D_h, hydraulic-weighted diameter.
Note: Values are mean ± SE. Nomenclature of species follows The Plant Lists (http://www.theplantlist.org/).

construct AI-VCs. Xylem embolism was induced by applying a series of increasing pressures using the pressure chamber after flushing the segments using 100 kPa KCl solution. A total of 8–10 pressurization treatments were applied to construct VCs for each segement (see Methods S2).

The pneumatic-air-discharge (PAD) method We used six branches of each species from different individuals to construct PAD-VCs following Pereira *et al.* (2016) and Zhang *et al.* (2018). Branches were rehydrated over a period of 2–3 h with all leaves bagged in black plastic bags. The distal 0.5 m to 1 m-long leafy parts were excised from the branches underwater and connected to a pneumatic apparatus (Pereira *et al.*, 2016) through a three-way valve connecting to a vacuum sensor (PX141-015V5V; Omega Engineering, Swedesboro, NJ, USA). The vacuum sensor was calibrated using a digital manometer (Xinsite HT-1895; Xinsite Technology Development Co., Ltd, Beijing, China) before taking measurements. We used a 5-mm-thick rigid silicone tube as a vacuum reservoir and a 100-ml syringe to create a vacuum pressure gradient (differential pressure against atmospheric pressure) of about −55 kPa. The pressure changes during the 2.5 min period immediately following the opening of the branch-reservoir valve were recorded using a datalogger (CR1000; Campbell Scientific, Logan, UT, USA). Using one fully dehydrated branch of each species prior to the PAD measurements, we determined the volume of the reservoir according to the branch size by changing the length of the reservoir tube to ensure that the final pressure gradient against atmospheric pressure ranged from −20 to −35 kPa. The extracted air (Δn_i; mol) was calculated as:

$$\Delta n_i = (P_f - P_i/\mathrm{RT}) \times 10^6, \quad \text{Eqn 3}$$

(P_f and P_i, initial and final pressures (kPa) during the 2.5 min extraction period immediately after opening the branch-reservoir valve; R, gas constant (8.314 kPa l mol^{-1} K^{-1}); and T, room temperature (°C)). During the experiment, the room temperature was maintained at 26°C using an air conditioner. The value Δn_i was converted to air volume (ΔV_i, μl) using ideal gas laws at atmospheric pressure: 95 kPa at 550 m asl in XTBG.

We conducted eight to ten repeat measurements for the same branch during slow dehydration under room conditions, and Ψ_{leaf} was periodically measured for each branch. The branches were treated as for the BD method to ensure leaf and stem equilibration then water potential was determined using bagged leaves (or terminal twigs). All cut surfaces were sealed with quick-drying glue. The leakage from the apparatus was estimated by the pressure change over the same time period (2.5 min) and subtracted from ΔV_i. We took two or three additional measurements after ΔV_i stopped increasing or even decreased.

The percentage of extracted air volume (PAD, %) from the branches was analogous to PLC (%) of hydraulic methods as:

$$\mathrm{PAD} = 100 \times (\Delta \mathrm{V}_i - \Delta \mathrm{V}_0)/(\Delta \mathrm{V}_{\max} - \Delta \mathrm{V}_0), \quad \text{Eqn 4}$$

(ΔV_0 (μl), air volume extracted from the fully hydrated branches initially; and $\Delta V_{\max}$, maximum air volume that can be extracted from the dehydrated stems).

The MicroCT imaging (MicroCT) method We performed MicroCT scans simultaneously with the BD method using a MicroCT system (SkyScan1275; Bruker Corporation, Billerica, MA, USA). Both ends of the branch segments (paired samples with the BD method) were recut underwater to *c.* 8 cm in length and connected with water-filled tubing (with a 1-cm-long water column). We tightly wrapped whole segments with parafilm to reduce dehydration during scanning. Compression was strictly avoided during the whole sample preparation process, and once prepared, segments were fixed vertically on the sample stage of the MicroCT system. To test whether embolism inside the segment was refilled when connected with water-filled tubing over time, we conducted a repeated scanning experiment for over 72 h before applying MicroCT to construct VCs for each species. We found no refilling of gas-filled vessels at least within the first 2 h; however, some gas-filled vessels were refilled with water after *c.* 4 h in two of the tested segments (Fig. S1).

At each stage of dehydration, we scanned twice to visualize gas-filled vessels and all vessels in the stem segments. Scans were performed at 36–50 kV and *c.* 200 μA energy at 5–8 μm voxel size depending on the diameter of the sample. Stem segments were scanned for 180° at a 0.2° rotation step and 1056 images were generated. Each scan took 12–18 min depending on the settings. The images were reconstructed and one slice at the middle position per segment was selected for analyses. Immediately after the first scan, we used 100 kPa compressed air to flush the stem segments. In a preliminary test, we found a 3–5 min air flushing from both ends of the segments was sufficient to ensure that all vessels were completely filled with air. Air-flushed segments were re-scanned following the same protocol described above to generate images showing all vessels in the same position. We estimated the theoretical hydraulic conductivity (K_t) for the two images of each sample according to the Hagen–Poiseuille equation:

$$K_t = (\rho \cdot \pi)/(128 \cdot \eta) \cdot \sum_{i=1}^{n} D_i^4, \quad \text{Eqn 5}$$

(ρ, water density (kg m^{-3}), η, water viscosity coefficient at a given temperature (MPa s); and D_i, conduit diameter (m) of embolized vessels).

We estimated the PLC (%) at each stage of dehydration as:

$$\mathrm{PLC} = 100 \times K_{t-i}/K_{t-\max}, \quad \text{Eqn 6}$$

($K_{t\text{-}i}$ and $K_{t\text{-max}}$, theoretical hydraulic conductivity of each stem segment before and after air flushing, respectively).

The optical (OP) method We constructed the OP-VCs for leaf midribs, which contain the closest xylem tissue in the laminar to the stem xylem. We scanned 6–12 leaves of each species. Branches were collected following the same protocol as described above for the BD method. The basal ends of the harvested

branches were recut underwater and rehydrated for 1–2 h in the laboratory until Ψ_{leaf} was close to 0 MPa. One healthy, mature leaf from each branch was placed under a stereomicroscope (M205A; Leica Microsystems, Wetzlar, Germany) and, following the protocol as described by Brodribb *et al.* (2016), grayscale images of the midribs were captured. The upper surface of each leaf was carefully fixed to the microscope stage using transparent double-sided adhesive tape. The illumination intensity was adjusted to make sure a clearly transmitted light image was visible under the stereomicroscope. Images of the midribs of each leaf were captured at 10-min intervals using a digital camera (DFC450; Leica Microsystems) attached to the microscope. We chose the midrib (first-order vein) as the region of interest because of the possibility of long vessels extending from the stem into the midrib and the potential lack of segmentation in vulnerability to embolism (Skelton *et al.*, 2017, 2018; Klepsch *et al.*, 2018; Lamarque *et al.*, 2018; Li *et al.*, 2020; Smith-Martin *et al.*, 2020). The OP method also has been used to scan stems (Brodribb *et al.*, 2017). However, it can only scan conduits on the surface, and debarking to expose xylem for scanning can result in the overestimation of vulnerability to embolism (Venturas *et al.*, 2019; notably a different image analysis method was used compared to Brodribb *et al.*, 2016a, 2017).

In order to monitor the water potential during dehydration, a small square of bark was removed from the stem adjacent to the targeted leaf to enable the installation of a PSY1 stem psychrometer (ICT International, Armidale, Australia) following Brodribb *et al.* (2017). The psychrometer was set to log at 10-min intervals. Measurements were taken for 3–5 d until the leaf samples were fully dehydrated and no more embolism events occurred. We maintained the room temperature at *c.* 26°C, and a 45% relative humidity under laboratory lighting. Because water loss occurs at very low rates after stomatal closure under room conditions, leaf and stem water potentials should equilibrate unless the leaves are completely isolated from the stems under high levels of embolism (Zhang & Brodribb, 2017). Moreover, given that Ψ_{leaf} is reported to decline linearly over time after stomatal closure (Brodribb *et al.*, 2016b), we were able to get a good estimation of Ψ_{leaf} at certain points in time.

We used an image subtraction method to estimate cumulative embolism throughout the midribs over time (Brodribb *et al.*, 2016b). The percentage of embolized area (PLA, %) was quantified as the ratio of embolized pixels at a given water potential to the numbers of embolized pixels at the fully embolized stage. Finally, 5–10 OP-VCs were constructed for each species.

Midday xylem tension and native embolism

We followed the protocol used by Chen *et al.* (2017) and Torres-Ruiz *et al.* (2015) to measure the native embolism of 1–2-yr-old stems during the 2019 dry season. Thereafter, we evaluated the differences between the directly measured native embolism levels and the predicted values from the laboratory determined VCs constructed using five different methods and water potential data. Six sun-exposed canopy branches per species were selected and marked one day before sampling. In addition, six fully expanded newest leaves from a neighboring branch were bagged with sealed bags and covered with aluminum foil on the previous evening. These leaf samples were harvested for water potential determination. We collected samples between 12:30 h and 13:30 h (solar time) from 23 to 25 March 2019. The branch samples (more than two times the MVLs) for PLC measurements were cut from the canopy using a 12-m-long pruner. The basal ends of the branches were wrapped with parafilm and the branches were sprayed with water and enclosed in black plastic bags. Samples were transported to the laboratory within 30 min. All samples were cut off 20 cm underwater from the base then kept in a dark room to release xylem tension (Wheeler *et al.*, 2013; Torres-Ruiz *et al.*, 2015) until $\Psi_{leaf} > -0.2$ MPa. The remaining segments were cut underwater to obtain two adjacent segments, each 10 cm in length (as described above for the BD method). These two segments were used for the determination of native PLC using both the hydraulic and MicroCT imaging methods, respectively. The native PLC was calculated as:

$$PLC = 100 \times (K_{max} - K_0)/K_{max}, \quad \text{Eqn 7}$$

(K_0 and K_{max}, native and maximum hydraulic conductances, respectively (determined using the hydraulic method), or the theoretical conductivity of visible vessels to all vessels in the cross-section, respectively (determined using the Micro-CT method)).

Finally, the MicroCT images scanned after air flushing were analyzed to determine hydraulic-weighted diameter ($D_h = \sum D^5 / \sum D^4$, μm) using IMAGE J software (National Institute of Health, New York, NY, USA) .

Data analysis

For each species, the percentage loss of hydraulic conductivity (BD, AI and MicroCT methods), percentage of extracted air volume (PAD method) and embolized area (OP method) derived from different methods were fitted against corresponding stem water potentials (applied pressures) using a sigmoid function (Pammenter & Vander Willigen, 1998). We applied a random intercept model for the OP data to account for the large variation among leaves (Fig. 1, right column). Based on the derived VCs, we calculated the water potentials (or applied pressure, P_{50}) at 50% loss of hydraulic conductivity (for BD, AI and MicroCT), 50% extracted air volume (for PAD) and 50% embolized area (for OP), and then compared P_{50} between methods using nonparametric bootstrap following Gauthey *et al.* (2020). Bootstrap 95% and 99.5% confidence intervals (CIs) for the predicted PLC and P_{50} were calculated using 2000 resamples. Because there were 10 method combinations for each species for P_{50} comparisons, 99.5% CIs were used to test for significant differences at the $P < 0.05$ level. All statistical analyses were conducted using R 3.6.3 (R Core Team, 2020) and the FITPLC package (Duursma & Choat, 2017).

Results

The MVLs of the five selected species ranged from relatively short vessels in *M. paniculate* (37.3 ± 2.6 cm) and

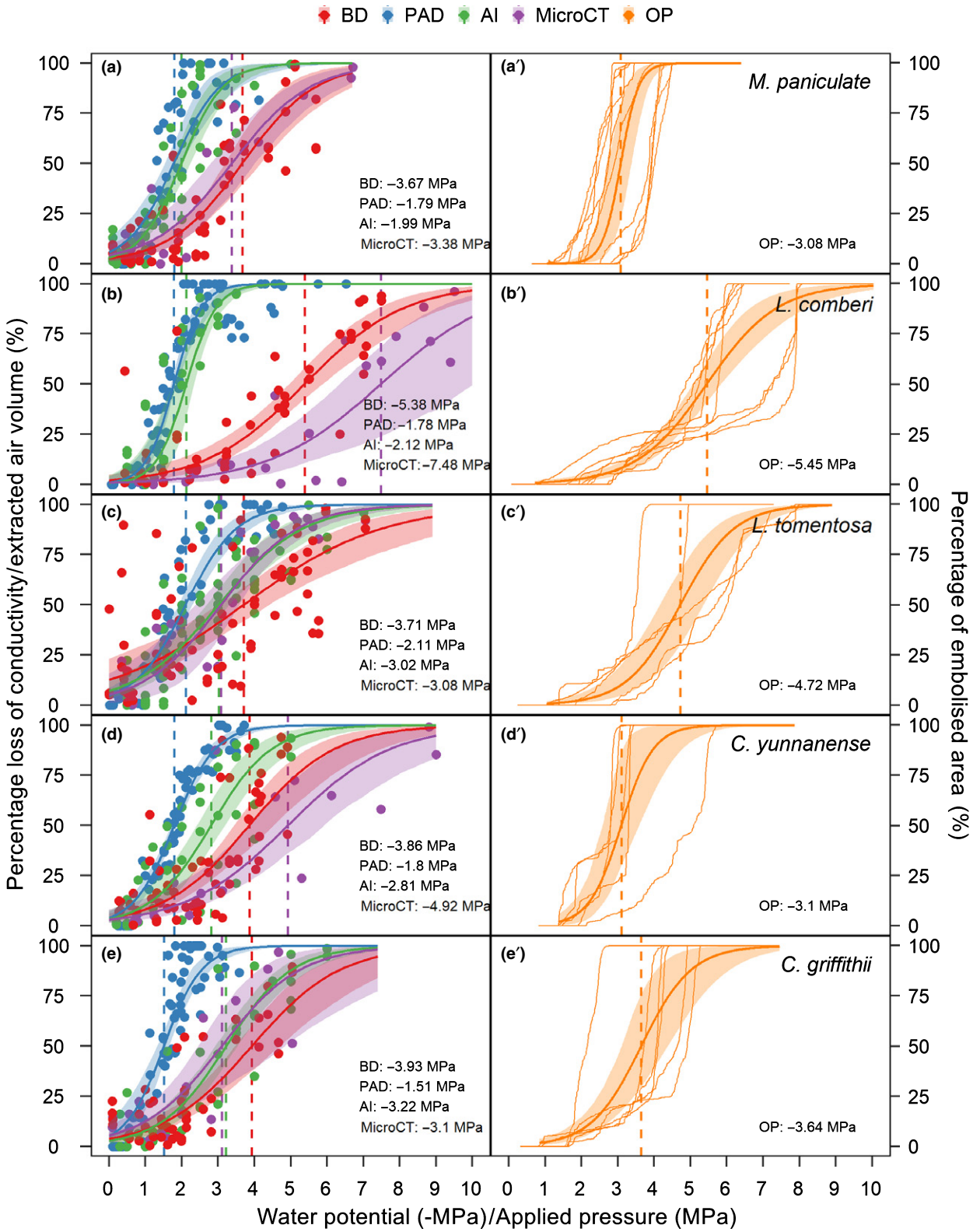

Fig. 1 Comparison of vulnerability curves (VCs) constructed using five different methods. BD, bench-top dehydration method (red symbol); PAD, pneumatic-air-discharge method (blue symbol); AI, air-injection-flow method (green symbol); MicroCT, MicroCT imaging method (purple symbol); OP, optical method (orange symbol, right column). The VCs were determined from branches using the BD, AI, PAD and MicroCT methods (left column, a–e) but from leaf midribs using the OP method (right column, a′–e′). For PAD method, the extracted air volume at the plateau 1 in Fig. 6 was used as V_{max}. Vertical dashed lines represent xylem water potentials at 50% loss of conductivity (for BD, AI and MicroCT), 50% extractable air volume (for PAD), and 50% embolized area (for OP), respectively. Regression lines are fitted by a three-parameter Sigmoid equation. The 95% confidence intervals are presented as shaded areas. *M. paniculate*, *Microcos paniculate*; *L. comberi*, *Lasiococca comberi*; *L. tomentosa*, *Lagerstroemia tomentosa*; *C. yunnanense*, *Combretum yunnanense*; *C. griffithii*, *Combretum griffithii*.

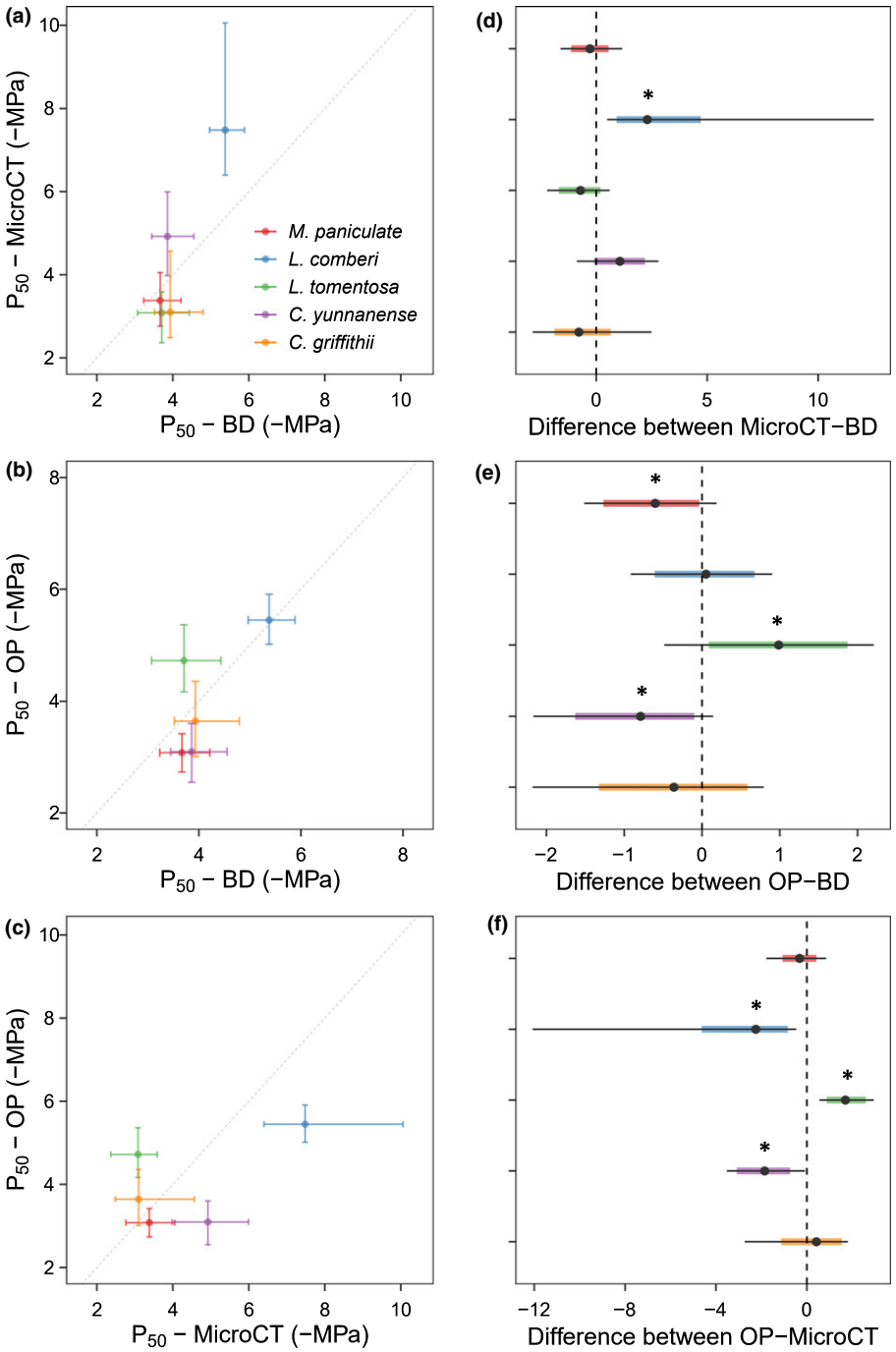

Fig. 2 Relationships between xylem water potentials at 50% loss of conductivity for the bench-top dehydration (P_{50}-BD) and MicroCT (P_{50}-MicroCT) methods, and 50% embolized area in leaf midrib for the optical methods (P_{50}-OP), respectively (a, b, c). Colored points represent mean P_{50} values estimated from sigmoidal fittings. Error bars indicate 95% confidence intervals (CIs) determined from 2000 nonparametric bootstraps. The dashed gray lines indicate 1 : 1 lines. CIs for difference between two methods (d–f). Black points, thick colored bars and thin gray bars represent means, 95% CIs and 99.5% CIs, respectively. If the 95% CIs overlap zero, then the two methods are not significantly different. Asterisks indicates the significant differences between methods. *M. paniculate*, *Microcos paniculate*; *L. comberi*, *Lasiococca comberi*; *L. tomentosa*, *Lagerstroemia tomentosa*; *C. yunnanense*, *Combretum yunnanense*; *C. griffithii*, *Combretum griffithii*.

L. comberi (39.3 ± 1.6 cm) to long vessels (> 120 cm) in *C. yunnanense* and *C. griffithii*. The D_h ranged from 53.73 ± 1.8 μm in *L. comberi* to 108.92 ± 10.0 μm in *C. griffithii* (Table 1).

Comparison of VCs among techniques

Although all VCs constructed using five techniques were S-shaped, generally, the VCs constructed using the BD, MicroCT

Table 2 Comparison of the mean P_{50} values derived from sigmoidal fittings.

Species	Method	P_{50} (95% CI) (MPa)
Microcos paniculate	BD	−3.67 (−4.22, −3.24) [c]
	PAD	−1.79 (−2.02, −1.55) [a]
	AI	−1.99 (−2.22, −1.76) [b]
	MicroCT	−3.38 (−4.03, −2.76) [b]
	OP	−3.08 (−3.40, −2.73) [b]
Lasiococca comberi	BD	−5.38 (−5.91, −4.99) [c]
	PAD	−1.78 (−1.87, −1.71) [a]
	AI	−2.12 (−2.36, −1.78) [b]
	MicroCT	−7.48 (−9.88, −6.36) [d]
	OP	−5.45 (−5.93, −5.05) [d]
Lagerstroemia tomentosa	BD	−3.71 (−4.38, −3.11) b
	PAD	−2.11 (−2.31, −1.91) [a]
	AI	−3.02 (−3.32, −2.71) [a]
	MicroCT	−3.08 (−3.63, −2.37) [a]
	OP	−4.72 (−5.36, −4.16) [c]
Combretum yunnanense	BD	−3.86 (−4.55, −3.44) [d]
	PAD	−1.80 (−1.88, −1.71) [a]
	AI	−2.81 (−3.17, −2.45) [b]
	MicroCT	−4.92 (−6.04, −3.94) [e]
	OP	−3.10 (−3.60, −2.55) [c]
Combretum griffithii	BD	−3.93 (−4.80, −3.51) [b]
	PAD	−1.51 (−1.66, −1.32) [a]
	AI	−3.22 (−3.52, −2.93) [a]
	MicroCT	−3.10 (−4.77, −2.48) [a]
	OP	−3.64 (−4.38, −2.98) [a]

BD, bench-top dehydration method; PAD, pneumatic-air-discharge method; AI, air-injection-flow method; MicroCT, X-ray-computed microtomography imaging method; OP, optical method; P_{50}, xylem water potentials at 50% loss of conductivity for the bench-top dehydration (BD, AI and MicroCT), 50% extracted air volume (PAD) and 50% embolized area in leaf midrib (OP), respectively. The VCs are from branches in the BD, AI, PAD and MicroCT methods, but from leaf midribs in the OP method. Confidence intervals (CIs) for P_{50} were determined from 2000 nonparametric bootstraps. Values in brackets are 95% CIs. P_{50} values sharing the same letters are not significantly different at the $P < 0.05$ level based on 99.5% CIs for differences between two methods. See Supporting Information Fig. S3 for 99.5% CIs.

and OP methods reached 100% PLC or embolism at more negative water potentials than those constructed using the AI and PAD methods. Both the BD and MicroCT methods produced more scattered PLC values than the other methods, which produced some high PLC values even at high (> −1 MPa) water potentials (Fig. 1).

There was considerable variation in P_{50} values produced by the five techniques for all five species (Figs 2, S2; Table 2). *Lasiococca comberi* showed the greatest variances in P_{50} among methods, ranging from −1.78 MPa (95% CI: −1.87, −1.71) produced by the PAD method to −7.48 MPa (95% CI: −10.06, −6.40) generated by the MicroCT method. However, the BD, MicroCT and OP methods generally produced comparable P_{50} values (Figs 2, S3; Table 2). There were discrepancies in P_{50} values produced by the MicroCT and BD methods but only for *L. comberi* (Figs 2, S2; Table 2). The PLC discrepancies between the BD and MicroCT methods increased against increasing embolism level, showing lower BD-PLCs than MicroCT-PLCs (Fig. S3). Among the methods, the most vulnerable VCs were derived from the PAD method. The AI method produced comparable P_{50} values for two of the five species but more negative P_{50} values for the other three compared to the PAD method (Figs 1, S2; Table 2). With reference to P_{50}-BD, the discrepancy ratios of P_{50}-AI but not P_{50}-PAD decreased with increasing MVL and D_h (Fig. 3). By contrast, the discrepancy ratios of P_{50}-AI and P_{50}-PAD against P_{50}-MicroCT were independent of xylem structural traits (Fig. S4).

Prediction of native xylem embolism using the five different methods

The five species showed a wide range in xylem tension during the dry season, with the minimum midday water potential varying from −0.99 MPa in *C. yunnanense* to −2.93 MPa in *L. comberi* (Fig. 4a). The observed PLCs *in situ* (measured hydraulically) ranged from 10.8 ± 5.5% in *C. griffithii* to 42.3 ± 10.8% in *L. tomentosa*. By contrast, the observed PLCs using MicroCT scanning ranged from 6.9 ± 1.3% in *C. griffithii* to 25.8 ± 9.3% in *L. tomentosa* (Fig. 4b). Generally, in most species, the PLCs predicted by BD-, MicroCT- and OP-produced VCs were lower than those predicted by the PAD- and AI-VCs.

The directly measured PLCs were comparable with the values predicted using the BD-VCs for three of the five species but lower in *L. tomentosa* and *C. yunnanense*. For *M. Paniculate*, *L. comberi* and *C. griffithii*, the PLCs predicted using the PAD-VCs were much higher than the directly measured values and those predicted using the other methods. Likewise, the PLCs predicted using the AI-VCs were higher than the measured PLCs for three of the five species but comparable in *C. griffithii* and *C. yunnanense*. The PLCs predicted from the MicroCT-VCs were similar to those from the OP-VCs (Fig. 4b).

Discussion

Our findings provide clear evidence that, for trees and lianas from tropical wet forests (known as long-vessel species), vulnerability curve (VC) characteristics strongly depend on the techniques that used. The maximum vessel lengths (MVLs) of all five species (37–141 cm) were distinctly longer than those of most species investigated in previous studies (0.015–66 cm; Pereira *et al.*, 2016; Zhang *et al.*, 2018; Venturas *et al.*, 2019). We found that the newly developed pneumatic-air-discharge (PAD) method tended to substantially overestimate the vulnerability of all five species included in this study, whereas the bench-top dehydration (BD), X-ray-computed microtomography (MicroCT) and optical (OP) methods yielded comparable P_{50} values. Moreover, the validity of the air-injection-flow (AI) method appears to be species-specific and its discrepancy against the BD method can be explained partly by the vessel length and diameter.

The underlying biases of different methods

The BD method generated S-shaped VCs for all species in this study, showing a general similarity with the VCs constructed

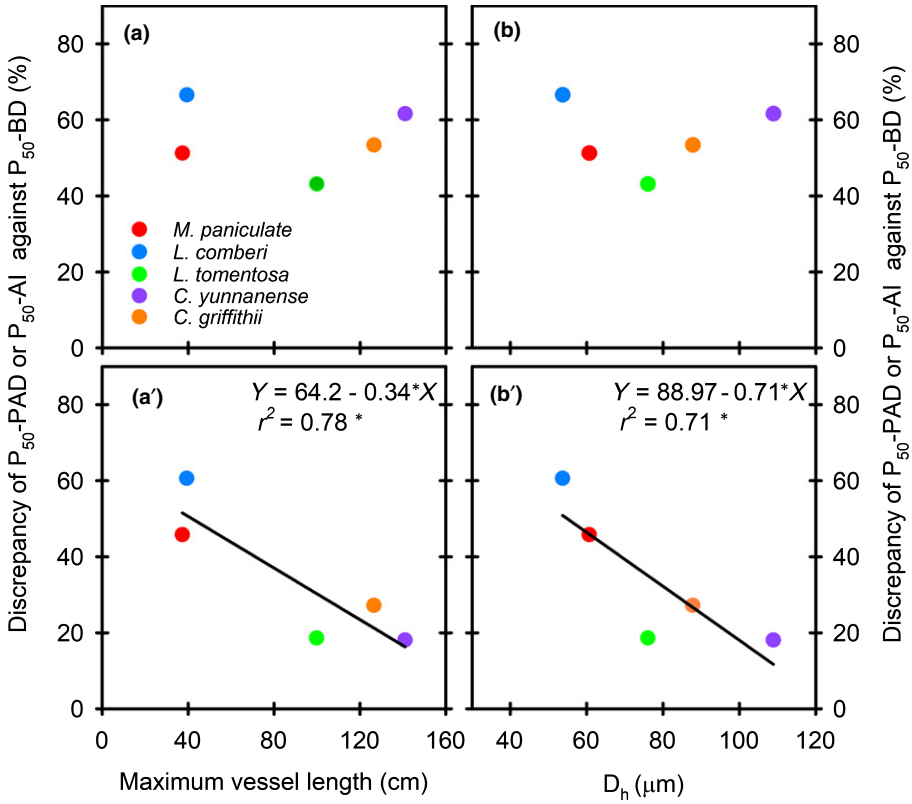

Fig. 3 The relationships between xylem structural traits and the discrepancy ratios (%) of P_{50}-PAD (a, b) and P_{50}-AI (a′, b′) against P_{50}-BD. P_{50}-PAD, xylem water potentials at 50% extractable air volume for PAD method; P_{50}-AI, applied pressure at 50% loss of conductivity for AI method; P_{50}-BD, xylem water potential at 50% loss of conductivity for BD method. PAD, pneumatic-air-discharge method; AI, air-injection-flow method, BD, the bench-top dehydration method; D_h, hydraulic-weighted diameter; solid lines are regression lines. *M. paniculate*, *Microcos paniculate*; *L. comberi*, *Lasiococca comberi*; *L. tomentosa*, *Lagerstroemia tomentosa*; *C. yunnanense*, *Combretum yunnanense*; *C. griffithii*, *Combretum griffithii*.

using the MicroCT and OP methods. In addition, the percentage losses of hydraulic conductance (PLCs) predicted from the BD-VCs and midday xylem tensions showed agreement with the directly measured PLCs. Notably, there were some high PLC values even under high water potentials (e.g. > -1.0 MPa; Fig. 1b–c) which did not match the MicroCT-generated PLCs, even when using neighboring segments from the same branch. Therefore, our results suggest the overall validity of the BD method for constructing VCs in tropical plants; however, the absolute PLC values of the BD-VCs should be interpreted with caution (Skelton & Diaz, 2020).

The reliability of the AI method is reported to be species-specific and prone to overestimating the vulnerability to embolism, especially for long-vessel species (Choat *et al.*, 2010; Ennajeh *et al.*, 2011; Martin-StPaul *et al.*, 2014). All segments analyzed in this study were much longer than the MVLs of the species and, hence, segment length could not account for why the AI method generated highly vulnerable VCs for the two short-vessel species (*Microcos paniculate* and *Lasiococca comberi*). However, we did find that the P_{50} discrepancy ratio of the AI against the BD method could be explained by vessel length and diameter (Figs 3, S4), which may be attributed to an 'effervescence' mechanism (Yin & Cai, 2018). Air bubbles may form in the water-filled vessels during the fast release of positive pressure after pressurization. This 'effervescence' effect may have different influences on long- and short-vessel species. Because long-vessel species possibly have greater numbers of longer vessels which are open from the pressurized part to the cut ends than short-vessel species, the air probably can flow out via the open ends of the cut vessels, resulting in less air dissolved in the sap water under the same pressure gradient. By contrast, short-vessel species can have more dissolved air in the sap under the same applied pressure because there is a higher resistance to air passing through entire closed vessels for a given length. Therefore, during the release of positive pressures, more air dissolved in the sap of short-vessel species could result in more 'effervescence' and higher PLCs compared with long-vessel species.

In this study, the PAD method consistently generated more vulnerable VCs for all five species than VCs produced using the BD, MicroCT and OP methods. Discrepancies in results between the PAD method and the other methods also have been found by a recent study in two conifers and three long-vessel angiosperms (Sergent *et al.*, 2020). We propose four mechanisms that may cause uncertainties in the PAD method. First, the PAD method may measure the vulnerability of only those vessels close to the cut end. These vessels are likely to be vulnerable because they are in direct contact with air sources. We found that extracting pressure cannot be detected at the distal ends when there are no cut vessels connecting both ends of the stem, suggesting that vacuum pressure that used to extract air from the xylem mainly extracts air from those cut vessels and vessels close to the cut end (Figs 5, S5–S8). This result corroborates the finding that air volume from distal end cavitated vessels isolated by water-filled intact vessels contributed little to extractable air volume (ΔV_i) (see Fig. S4 in Pereira *et al.*, 2016). Therefore, the VCs produced by the PAD method probably represent the vulnerability of neighboring vessels of cut ones, and the embolized cut vessels are likely to make the neighboring vessels more susceptible to embolism. This may occur according to the 'air-seeding'

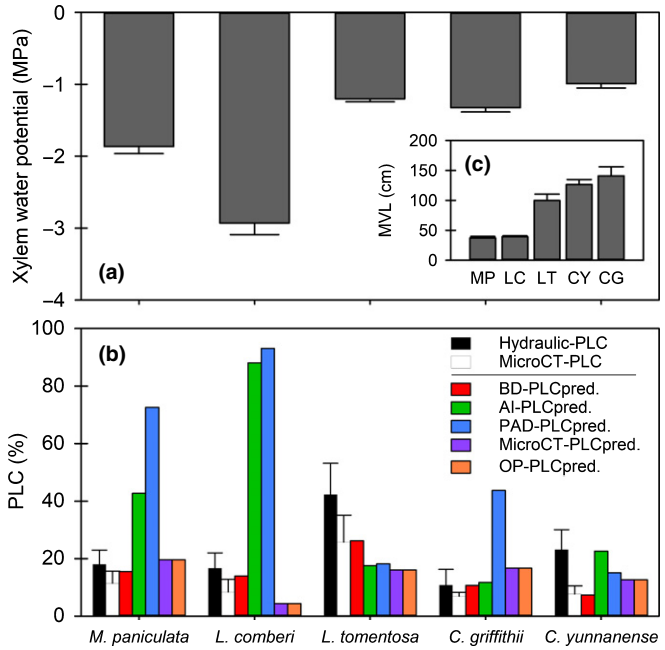

Fig. 4 The minimum midday xylem water potential (a, values are mean ± SE) and the percentage loss of conductivity (PLC) (b, values are mean ± SE). In (b), bars are directly measured values *in situ* using the hydraulic meauements (Hydraulic-PLC, black solid), directly measured values using the MicroCT imaging (MicroCT-PLC, white bar) and values predicted ($PLC_{pred.}$) from vulnerability curves constructed using five different methods and xylem water potential. Different color bars indicate values from different methods, as indicated in the figure. BD, bench-top dehydration method; PAD, pneumatic-air-discharge method; AI, air-injection-flow method; MicroCT, MicroCT imaging method; OP, optical method. Inset (c) shows the maximum vessel length (MVL, values are mean ± SE) for each species. MP, *Microcos paniculate*; LC, *Lasiococca comberi*; LT, *Lagerstroemia tomentosa*; CY, *Combretum yunnanense*; CG, *Combretum griffithii*.

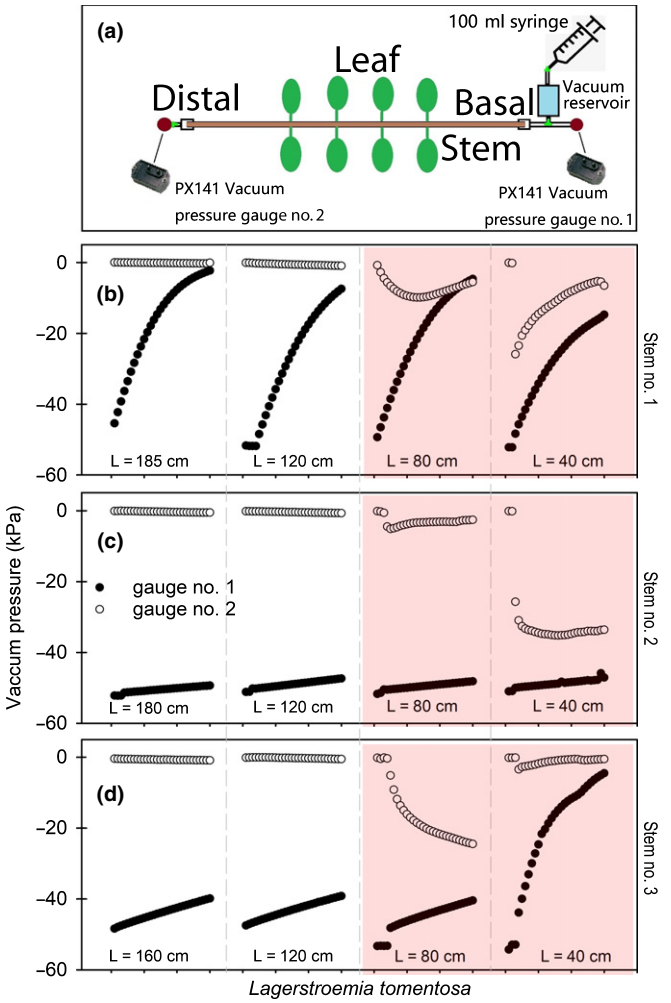

Fig. 5 Diagram of the pneumatic-air-discharge apparatus for testing the sample length effect (a) and the differential vacuum pressure changes over 2.5 min for samples with different sample-length spans for three stems of *Lagerstroemia tomentosa* (b–d). Closed and open symbols in (b–d) represent the vacuum pressure at the basal (gauge no. 1) and the distal (gauge no. 2) ends, respectively. The red shadows highlight when the sample length (L, cm) being shorter than the maximum vessel length of the segment.

hypothesis because the pits of the neighboring vessels are in direct contact with emboli (Zimmermann, 1983; Christman *et al.*, 2009).

Secondly, there are uncertainties in estimating the maximum extractable air volume (ΔV_{max}) and percentage embolism. In an additional test using *L. comberi* (Methods S3), we found two pronounced plateaus of ΔV_i in all six branches during the dehydration process (Fig. 6). Distal embolized vessels, which were not connected to the cut-open vessels via embolized vessels (Fig. S9b), were excluded from the estimation because air cannot be extracted from them (the first plateau in Fig. 6). The high vulnerability of the vessels neighboring the cut ones (as discussed above) could explain why the PAD method generated more vulnerable VCs than the other methods. The second plateau suggested that the ΔV_{max} was from all vessels (Fig. S9c) and potential cracks in the pith and xylem tissues. In this case, the embolism level might have been substantially underestimated for stages under moderate dehydration owing to exclusion of the distal embolized vessels. The selection of ΔV_{max} from different plateaus generated a four-fold difference in P_{50} (−1.58 vs −6.32 MPa; Fig. 6c).

Thirdly, there are uncertainties regarding the source of the air. Pereira *et al.* (2020) showed a stable ΔV_{max} in *Citrus sinensis* after all vessels were fully cavitated. However, the ΔV_{max} may include substantial air volume from outside the vessels, especially for species with a large pith and/or high parenchyma fraction in the xylem, which would potentially crack under desiccation. The MicroCT images of samples in different dehydration stages showed evidence of cracks both in the pith and xylem tissue during the dehydration process. Air also may be extracted from these areas external to the vessels and calculated as part of the air volume from cavitated vessels. Moreover, the extent of cracking during dehydration differed among species. For example, species with a large pith fraction were prone to crack during desiccation. In this study, *Combretum griffithii* showed cracks in the pith when the xylem water potential decreased to −3.48 MPa. By contrast, no cracks were detected in *L. comberi* (Fig. 7). In another test, we found that there was an further increase in

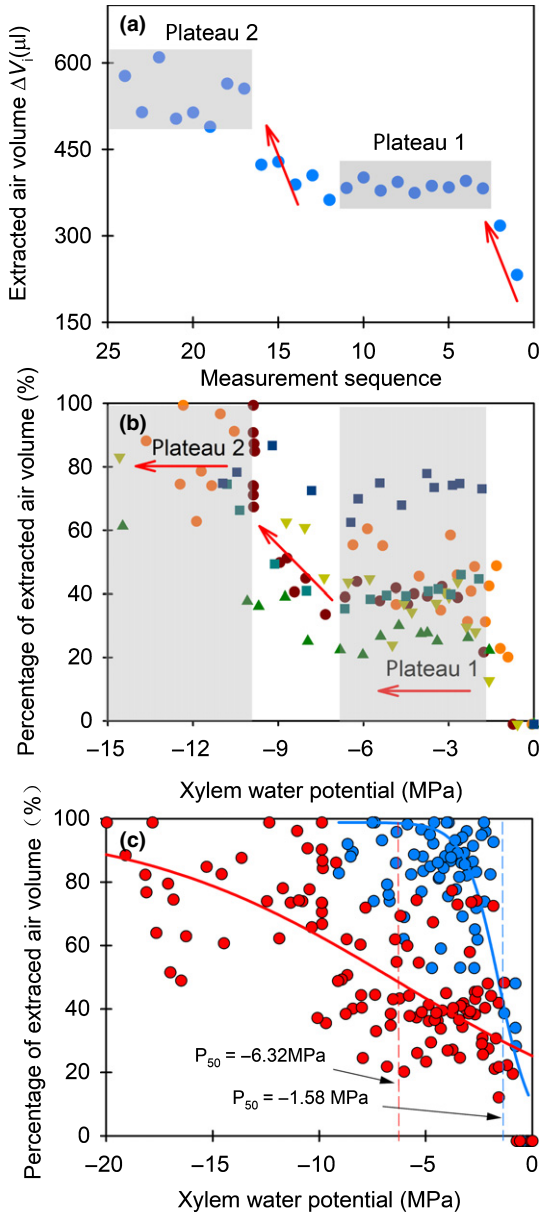

Fig. 6 The kinetics of extracted air volume (ΔV_i, μl) (a) of one representative stem sample of *Lasiococca comberi* using the pneumatic-air-discharge (PAD) method; (b) percentage of extractable air volume against xylem water potential for different stem segments; and (c) comparison of the PAD method vulnerability curves (VCs) using the maximum extractable air volume at plateaus 1 (blue) and 2 (red), respectively, in *Lasiococca comberi*. Symbols of different colors in (b) represent different stem samples (n = 6 stems). The gray areas indicate two plateau stages (when a stable extractable air volume was reached) during the drying process. Data from six stems were pooled together in (c) to construct the VCs. Vertical dashed lines in (c) represent the xylem water potential at 50% extracted air volume (P_{50}).

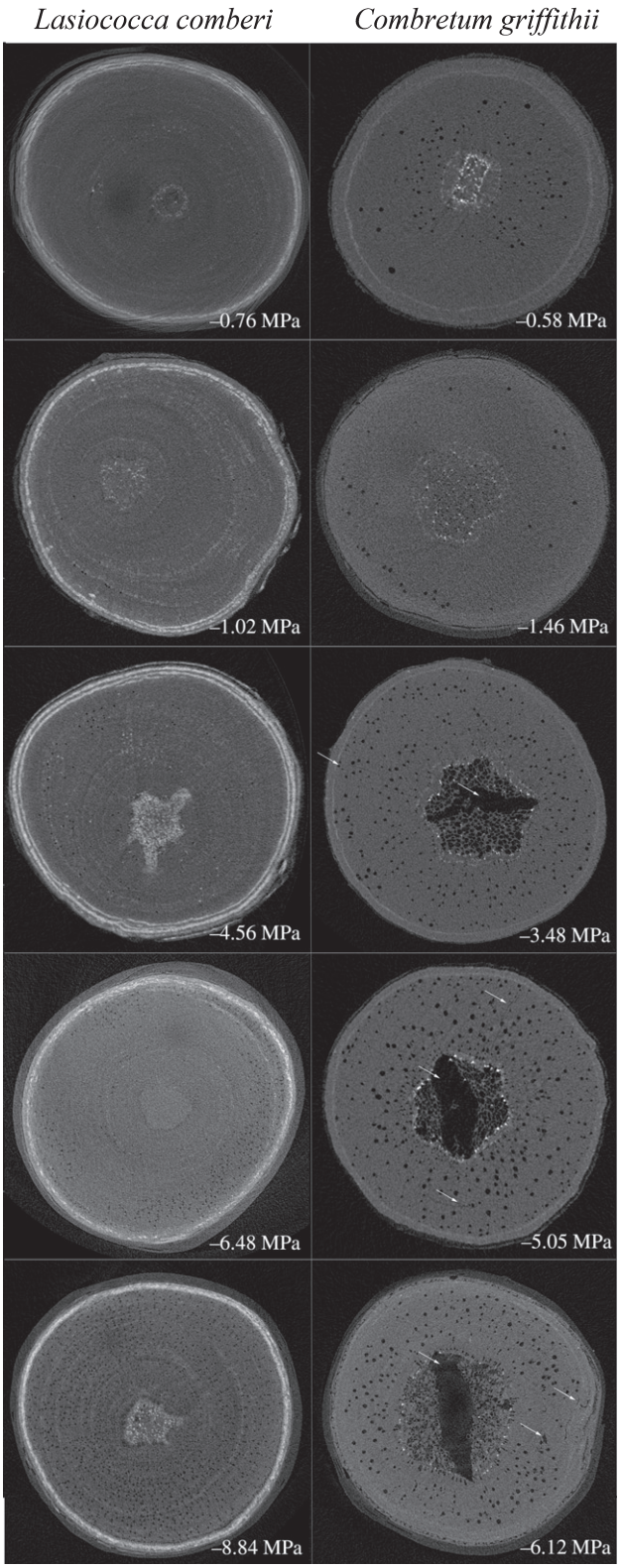

Fig. 7 MicroCT images of stems at different desiccation stages for *Lasiococca comberi* (left column) and *Combretum griffithii* (right column). Numbers are xylem water potentials. The arrows indicate cracks in the pith and xylem tissue.

extracted air volume after vessels were fully embolized by pressurization in two species with a large pith: *C. griffithii* (*c.* 33%) and *Bauhinia tenuiflora* (*c.* 28%; Y.J. Chen *et al.* unpublished).

Fourthly, there is a shrinkage effect that may have influenced the validity of the PAD method. In *C. griffithii* and *B. tenuiflora*, we found that tissue shrinkage due to dehydration caused a decline of *c.* 36.6% and 40.65% in phloem area, 11.9% and

30.9% in xylem area, 11.9% and 30.9% in pith area, and, by contrast, an increase of 8.1% and 3.5% in vessel lumen area, respectively (Fig. S10).

Taking these four mechanisms with opposite effects together, the resultant VCs may depend largely on which mechanism dominates as the main effect. In the present study, the first mechanism may dominate, resulting in more vulnerable VCs. Therefore, although PAD is a low-cost and experimentally simple method, it should be used cautiously owing to these uncertainties.

We found that the MicroCT-VCs and OP-VCs generally matched the BD-VCs in most species, showing high resistant VCs (Fig. 2). Our findings are consistent with Losso *et al.* (2019) that PLCs derived from hydraulic measurements closely matched the MicroCT-PLCs. We also noted great intraspecific differences when using the OP method, which is consistent with previous studies (Fig. 1; Rodriguez-Dominguez *et al.*, 2018; Cardoso *et al.*, 2020; Gauthey *et al.*, 2020). Although previous studies showed that the MicroCT method tended to generate more resistant VCs compared to the BD method (Lopez *et al.*, 2019), this was only evident in *L. comberi*. Therefore, we conclude, along with Gauthey *et al.* (2020), that these visual techniques provide promising estimates of xylem cavitation resistance. However, the MicroCT and OP methods also may be associated with potential errors and artifacts produced during experiments or through the way the images are converted into the levels of xylem dysfunction. Caution is needed when using these two methods to estimate the absolute value of conductivity because both methods actually estimate 2D embolism pixels or theoretical values based on lumen diameters but ignore the resistance of the other components in the vessels, such as pits and end walls (Gauthey *et al.*, 2020).

The application of VCs generated using different methods confound the predicted performance in ecological research

In our study, the highly vulnerable VCs constructed using the AI and PAD methods indicate that cavitation occurs routinely in the focal plants; however, this finding contradicts our understanding of plant hydraulic performance in the field. Our findings suggest that methodological issues can result in incorrect explanations of plant physiological performance and ecological adaptations. For instance, *L. comberi* is one of the most dominant evergreen species in the tropical limestone forests of the study region where severe water stress occurs frequently during the dry seasons (Chen *et al.*, 2015). Previous studies have shown high xylem vulnerability to embolism in this species using the AI method including $P_{50} = -1.66$ MPa in Fu *et al.* (2012), and $P_{50} = -2.0$ MPa in Zhu *et al.* (2017). This also was the case in the present study ($P_{50} = -1.78$ MPa). However, this species experienced rather low water potentials during the dry season: −3.77 MPa in Fu *et al.* (2012), −6.58 MPa in Chen *et al.* (2015) and −2.92 MPa in this study. Interestingly, whole-plant mortality or branch dieback of this species is rarely observed in the field which is inconsistent with the predictions based on the AI-VCs or PAD-VCs that suggest full (100%) xylem embolism. If the AI- and PAD-VCs are accurate, the existence of novel embolism-refilling mechanisms is essential for the survival and ecological dominance of this species in tropical limestone forests. However, routine daily cycles of embolism-formation and night-refilling have not been confirmed in many studies (Charrier *et al.*, 2016; Lamarque *et al.*, 2018). We propose that the VCs generated using the BD, MicroCT and OP methods (Fig. 4) can better explain the dominance of this species and absence of dry season branch or tree dieback without the need for novel embolism-refilling mechanisms.

Because of the methodological issues related to how VCs are generated, methods and experimental protocols have been a major concern for many years (Cochard *et al.*, 2013). The insight that there is a convergence in the vulnerability of forests to drought (Choat *et al.*, 2012; Anderegg *et al.*, 2019) may need to be revisited in consideration of the great uncertainties about P_{50} in the literature. In this study, we found that the VCs generated using the BD (with tensions relaxed before hydraulic measurements), MicroCT and OP methods were generally similar and could predict the performance of the plants in the field. By contrast, the AI and PAD methods showed a number of uncertainties. Whereas overestimation of vulnerability to embolism, predicted by vessel size, occurs for the AI method, the uncertainties associated with the PAD method can result in either an overestimate or underestimate of the vulnerability. Our findings highlight the need for caution when using VCs to explain or predict plant responses to drought or drought-induced tree mortality under future climate change scenarios.

Acknowledgments

The authors thank Song Lv, Peifu Li and Hong Ma for field support, Kyle Tomlinson for data analysis, Abby Novak for language editing, Xin Jia for drawing the gas kinetics diagram in Fig S9, Aldous Hofmann and Marlys Rietdyk for OP image analyses. This work was funded by the National Natural Science Foundation of China (41861144016, 31570406, 31861133008), Youth Innovation Promotion Association (2016351) and the 'Light of West China' Program of CAS, the CAS 135 program (2017XTBG-T01, 2017XTBG-F01), Yunnan Provincial Science and Technology Department (2018HB068). PM acknowledges financial support from CAS-TWAS President's Fellowship for International Doctoral Students. ZYJ acknowledges financial support from the open fund of CAS Key Laboratory of Tropical Forest Ecology. MK acknowledges CAS President's International Fellowship Initiative (2020FYB0003).

Author contributions

Y-JC conceived and designed this study; Y-JC, PM, HG, L-BT and SK performed experiments; Y-JC, PM, KB, MK, Y-JZ and J-LZ analyzed the data; and Y-JC wrote and revised the manuscript with input from PM, Y-JZ, KB and J-LZ. Y-JC and PM contributed equally to this work.

ORCID

Ya-Jun Chen https://orcid.org/0000-0001-5753-5565
Sasiwimol Kaewkamol https://orcid.org/0000-0002-9909-9252
Masatoshi Katabuchi https://orcid.org/0000-0001-9900-9029
Phisamai Maenpuen https://orcid.org/0000-0002-0441-6367
Jiao-Lin Zhang https://orcid.org/0000-0003-3693-7965
Yong-Jiang Zhang https://orcid.org/0000-0001-5637-3015

References

Alder NN, Pockman WT, Sperry J, Nuismer S. 1997. Use of centrifugal force in the study of xylem cavitation. *Journal of Experimental Botany* **48**: 665–674.

Allen CD, Macalady AK, Chenchouni H, Bachelet D, McDowell N, Vennetier M, Kitzberger T, Rigling A, Breshears DD, Hogg EH *et al.* 2010. A global overview of drought and heat-induced tree mortality reveals emerging climate change risks for forests. *Forest Ecology and Management* **259**: 660–684.

Anderegg WRL, Anderegg LDL, Kerr KL, Trugman AT. 2019. Widespread drought-induced tree mortality at dry range edges indicates that climate stress exceeds species' compensating mechanisms. *Global Change Biology* **25**: 3793–3802.

Anderegg WR, Berry JA, Field CB. 2012. Linking definitions, mechanisms, and modeling of drought-induced tree death. *Trends in Plant Science* **17**: 693–700.

Anderegg WR, Klein T, Bartlett M, Sack L, Pellegrini AF, Choat B, Jansen S. 2016. Meta-analysis reveals that hydraulic traits explain cross-species patterns of drought-induced tree mortality across the globe. *Proceedings of the National Academy of Sciences, USA* **113**: 5024–5029.

Anderegg WRL, Konings AG, Trugman AT, Yu K, Bowling DR, Gabbitas R, Karp DS, Pacala S, Sperry JS, Sulman BN *et al.* 2018. Hydraulic diversity of forests regulates ecosystem resilience during drought. *Nature* **561**: 538–541.

Brodersen CR, McElrone AJ, Choat AJ, Matthews MA, Shackel MA. 2010. The dynamics of embolism repair in xylem: *In vivo* visualizations using high-resolution computed tomography. *Plant Physiology* **154**: 1088–1095.

Brodribb TJ, Bienaime D, Marmottant P. 2016a. Revealing catastrophic failure of leaf networks under stress. *Proceedings of the National Academy of Sciences, USA* **113**: 4865–4869.

Brodribb TJ, Carriqui M, Delzon S, Lucani C. 2017. Optical measurement of stem xylem vulnerability. *Plant Physiology* **174**: 2054–2061.

Brodribb TJ, Skelton RP, McAdam SA, Bienaime D, Lucani CJ, Marmottant P. 2016b. Visual quantification of embolism reveals leaf vulnerability to hydraulic failure. *New Phytologist* **209**: 1403–1409.

Cai J, Li S, Zhang H, Zhang S, Tyree MT. 2014. Recalcitrant vulnerability curves: methods of analysis and the concept of fibre bridges for enhanced cavitation resistance. *Plant, Cell & Environment* **37**: 35–44.

Cao M, Zou XM, Warren M, Zhu H. 2006. Tropical forests of Xishuangbanna, China. *Biotropica* **38**: 306–309.

Cardoso AA, Batz TA, McAdam SAM. 2020. Xylem embolism resistance determines leaf mortality during drought in *Persea americana*. *Plant Physiology* **182**: 547–554.

Charrier G, Torres-Ruiz JM, Badel E, Burlett R, Choat B, Cochard H, Delmas CEL, Domec JC, Jansen S, King A *et al.* 2016. Evidence for hydraulic vulnerability segmentation and lack of xylem refilling under tension. *Plant Physiology* **172**: 1657–1668.

Chen YJ, Cao KF, Schnitzer SA, Fan ZX, Zhang JL, Bongers F. 2015. Water-use advantage for lianas over trees in tropical seasonal forests. *New Phytologist* **205**: 128–136.

Chen YJ, Schnitzer SA, Zhang YJ, Fan ZX, Goldstein G, Tomlinson KW, Lin H, Zhang JL, Cao KF. 2017. Physiological regulation and efficient xylem water transport regulate diurnal water and carbon balances of tropical lianas. *Functional Ecology* **31**: 306–317.

Choat B, Badel E, Burlett R, Delzon S, Cochard H, Jansen S. 2016. Noninvasive measurement of vulnerability to drought-induced embolism by X-ray microtomography. *Plant Physiology* **170**: 273–282.

Choat B, Brodribb TJ, Brodersen CR, Duursma RA, Lopez R, Medlyn BE. 2018. Triggers of tree mortality under drought. *Nature* **558**: 531–539.

Choat B, Drayton WM, Brodersen C, Matthews MA, Shackel KA, Wada H, Mcelrone AJ. 2010. Measurement of vulnerability to water stress-induced cavitation in grapevine: a comparison of four techniques applied to a long-vesseled species. *Plant, Cell & Environment* **33**: 1502–1512.

Choat B, Jansen S, Brodribb TJ, Cochard H, Delzon S, Bhaskar R, Bucci SJ, Feild TS, Gleason SM, Hacke UG *et al.* 2012. Global convergence in the vulnerability of forests to drought. *Nature* **491**: 752–755.

Christman MA, Sperry JS, Adler FR. 2009. Testing the 'rare pit' hypothesis for xylem cavitation resistance in three species of *Acer*. *New Phytologist* **182**: 664–674.

Cochard H, Badel E, Herbette S, Delzon S, Choat B, Jansen S. 2013. Methods for measuring plant vulnerability to cavitation: a critical review. *Journal of Experimental Botany* **64**: 4779–4791.

Cochard H, Cruiziat P, Tyree MT. 1992. Use of positive pressures to establish vulnerability curves. *Plant Physiology* **100**: 205–209.

Cochard H, Damour G, Bodet C, Tharwat I, Poirier M, Ameglio T. 2005. Evaluation of a new centrifuge technique for rapid generation of xylem vulnerability curves. *Physiologia Plantarum* **124**: 410–418.

Cochard H, Delzon S, Badel E. 2015. X-ray microtomography (micro-CT): a reference technology for high-resolution quantification of xylem embolism in trees. *Plant, Cell & Environment* **38**: 201–206.

Cochard H, Herbette S, Barigah T, Badel E, Ennajeh M, Vilagrosa A. 2010. Does sample length influence the shape of xylem embolism vulnerability curves? A test with the Cavitron spinning technique. *Plant, Cell & Environment* **33**: 1543–1552.

Dixon HH, Joly J. 1895. On the ascent of sap. *Philosophical Transactions of the Royal Society of London. Series B: Biological Sciences* **186**: 563–576.

Duursma RA, Choat B. 2017. fitplc – an R package to fit hydraulic vulnerability curves. *Journal of Plant Hydraulics* **4**: e-002.

Ennajeh M, Simoes F, Khemira H, Cochard H. 2011. How reliable is the double-ended pressure sleeve technique for assessing xylem vulnerability to cavitation in woody angiosperms? *Physiologia Plantarum* **142**: 205–210.

Ewers FW, Fisher JB. 1987. A survey of vessel lengths and diameters in stems of some tropical lianas. *American Journal of Botany* **74**: 613.

Fu PL, Jiang YJ, Wang AY, Brodribb TJ, Zhang JL, Zhu SD, Cao KF. 2012. Stem hydraulic traits and leaf water-stress tolerance are co-ordinated with the leaf phenology of angiosperm trees in an Asian tropical dry karst forest. *Annals of Botany* **110**: 189–199.

Gambetta GA, Herrera JC, Dayer S, Feng Q, Hochberg U, Castellarin SD. 2020. Grapevine drought stress physiology: towards an integrative definition of drought tolerance. *Journal of Experimental Botany* **71**: 4658–4676.

Gao H, Chen YJ, Zhang YJ, Maenpuen P, Lv S, Zhang JL. 2019. Vessel-length determination using silicone and air injection: are there artifacts? *Tree Physiology* **39**: 1783–1791.

Gauthey A, Peters JMR, Carins-Murphy MR, Rodriguez-Dominguez CM, Li X, Delzon S, King A, Medlyn BE, Tissue DT, Brodribb TJ *et al.* 2020. Evaluating methods used to measure cavitation resistance in seven woody species with differing xylem anatomy: a comparison of visual and hydraulic techniques. *New Phytologist* 228: 884–897.

Jacobsen AL, Pratt RB, Tobin MF, Hacke UG, Ewers FW. 2012. A global analysis of xylem vessel length in woody plants. *American Journal of Botany* **99**: 1583–1591.

Jansen S, Schuldt B, Choat B. 2015. Current controversies and challenges in applying plant hydraulic techniques. *New Phytologist* **205**: 961–964.

Klepsch M, Zhang Y, Kotowska MM, Lamarque LJ, Nolf M, Schuldt B, Torres-Ruiz JM, Qin DW, Choat B, Delzon S *et al.* 2018. Is xylem of angiosperm leaves less resistant to embolism than branches? Insights from microCT, hydraulics, and anatomy. *Journal of Experimental Botany* **69**: 5611–5623.

Lamarque LJ, Corso D, Torres-Ruiz JM, Badel E, Brodribb TJ, Burlett R, Charrier G, Choat B, Cochard H, Gambetta GA *et al.* 2018. An inconvenient truth about xylem resistance to embolism in the model species for refilling *Laurus nobilis* L. *Annals of Forest Science* **75**: 88.

Li X, Delzon S, Torres-Ruiz J, Badel E, Burlett R, Cochard H, Jansen S, King A, Lamarque LJ, Lenoir N *et al.* 2020. Lack of vulnerability segmentation in four angiosperm tree species: evidence from direct X-ray microtomography observation. *Annals of Forest Science* **77**: 37.

Lopez R, Nolf M, Duursma RA, Badel E, Flavel RJ, Cochard H, Choat B. 2019. Mitigating the open vessel artefact in centrifuge-based measurement of embolism resistance. *Tree Physiology* **39**: 143–155.

Losso A, Bar A, Damon B, Dullin C, Ganthaler A, Petruzzellis F, Savi T, Tromba G, Nardini A, Mayr S *et al.* 2019. Insights from in vivo micro-CT analysis: testing the hydraulic vulnerability segmentation in *Acer pseudoplatanus* and *Fagus sylvatica* seedlings. *New Phytologist* **221**: 1831–1842.

Martin-StPaul NK, Longepierre D, Huc R, Delzon S, Burlett R, Joffre R, Rambal S, Cochard H. 2014. How reliable are methods to assess xylem vulnerability to cavitation? The issue of 'open vessel' artifact in oaks. *Tree Physiology* **34**: 894–905.

McDowell N, Pockman WT, Allen CD, Breshears DD, Cobb N, Kolb T, Plaut J, Sperry J, West A, Williams DG *et al.* 2008. Mechanisms of plant survival and mortality during drought: why do some plants survive while others succumb to drought? *New Phytologist* **178**: 719–739.

McDowell NG. 2011. Mechanisms linking drought, hydraulics, carbon metabolism, and vegetation mortality. *Plant Physiology* **155**: 1051–1059.

Milburn JA, Johnson RPC. 1966. Conduction of sap: II. Detection of vibrations produced by sap cavitation in *Ricinus* xylem. *Planta* **69**: 43–52.

Pammenter NW, Vander Willigen C. 1998. A mathematical and statistical analysis of the curves illustrating vulnerability of xylem to cavitation. *Tree Physiology* **18**: 589–593.

Pereira L, Bittencourt PR, Oliveira RS, Junior MB, Barros FV, Ribeiro RV, Mazzafera P. 2016. Plant pneumatics: stem air flow is related to embolism - new perspectives on methods in plant hydraulics. *New Phytologist* **211**: 357–370.

Pereira L, Bittencourt PRL, Pacheco VS, Miranda MT, Zhang Y, Oliveira RS, Groenendijk P, Machado EC, Tyree MT, Jansen S *et al.* 2020. The Pneumatron: An automated pneumatic apparatus for estimating xylem vulnerability to embolism at high temporal resolution. *Plant, Cell & Environment* **43**: 131–142.

Pratt RB, Castro V, Fickle JC, Jacobsen AL. 2020. Embolism resistance of different aged stems of a California oak species (*Quercus douglasii*): optical and microCT methods differ from the benchtop-dehydration standard. *Tree Physiology* **40**: 5–18.

R Core Team. 2020. *R: a language and environment for statistical computing*, v. 3.6.3. Vienna, Austria: R Foundation for Statistical Computing. [WWW document] URL https://www.R-project.org

Reichstein M, Bahn M, Ciais P, Frank D, Mahecha MD, Seneviratne SI, Zscheischler J, Beer C, Buchmann N, Frank DC *et al.* 2013. Climate extremes and the carbon cycle. *Nature* **500**: 287–295.

Rockwell FE, Wheeler JK, Holbrook NM. 2014. Cavitation and its discontents: opportunities for resolving current controversies. *Plant Physiology* **164**: 1649–1660.

Rodriguez-Dominguez CM, Carins Murphy MR, Lucani C, Brodribb TJ. 2018. Mapping xylem failure in disparate organs of whole plants reveals extreme resistance in olive roots. *New Phytologist* **218**: 1025–1035.

Sergent AS, Varela SA, Barigah TS, Badel E, Cochard H, Dalla-Salda G, Delzon S, Fernández ME, Guillemot J, Gyenge J *et al.* 2020. A comparison of five methods to assess embolism resistance in trees. *Forest Ecology and Management* **468**: 118175.

Skelton RP, Brodribb TJ, Choat B. 2017. Casting light on xylem vulnerability in an herbaceous species reveals a lack of segmentation. *New Phytologist* **214**: 561–569.

Skelton RP, Dawson TE, Thompson SE, Shen Y, Weitz AP, Ackerly D. 2018. Low vulnerability to xylem embolism in leaves and stems of north American oaks. *Plant Physiology* **177**: 1066–1077.

Skelton R, Diaz J. 2020. Quantifying losses of plant hydraulic function: seeing the forest, the trees and the xylem. *Tree Physiology* **40**: 285–289.

Skelton RP, West AG, Dawson TE. 2015. Predicting plant vulnerability to drought in biodiverse regions using functional traits. *Proceedings of the National Academy of Sciences, USA* **112**: 5744–5749.

Smith-Martin CM, Skelton RP, Johnson KM, Lucani C, Brodribb TJ, Sala A. 2020. Lack of vulnerability segmentation among woody species in a diverse dry sclerophyll woodland community. *Functional Ecology* **34**: 777–787.

Sperry J. 2013. Cutting-edge research or cutting-edge artefact? An overdue control experiment complicates the xylem refilling story. *Plant, Cell & Environment* **36**: 1916–1918.

Sperry JS, Donnelly JR, Tyree MT. 1988. A method for measuring hydraulic conductivity and embolism in xylem. *Plant, Cell & Environment* **11**: 35–40.

Sperry JS, Tyree MT. 1990. Water-stress-induced xylem embolism in three species of conifers. *Plant, Cell & Environment* **13**: 427–436.

Torres-Ruiz JM, Jansen S, Choat B, McElrone AJ, Cochard H, Brodribb TJ, Badel E, Burlett R, Bouche PS, Brodersen CR *et al.* 2015. Direct X-ray microtomography observation confirms the induction of embolism upon xylem cutting under tension. *Plant Physiology* **167**: 40–43.

Tyree MT, Ewers F. 1991. The hydraulic architecture of trees and other woody plants. *New Phytologist* **119**: 345–360.

Tyree MT, Zimmermann MH. 2002. *Xylem structure and the ascent of sap*. Berlin, Germany: Springer.

Venturas MD, Pratt RB, Jacobsen AL, Castro V, Fickle JC, Hacke UG. 2019. Direct comparison of four methods to construct xylem vulnerability curves: differences among techniques are linked to vessel network characteristics. *Plant, Cell & Environment* **42**: 2422–2436.

Venturas MD, Sperry JS, Hacke UG. 2017. Plant xylem hydraulics: what we understand, current research, and future challenges. *Journal of Integrative Plant Biology* **59**: 356–389.

Wang R, Zhang L, Zhang S, Cai J, Tyree MT. 2014. Water relations of *Robinia pseudoacacia* L.: do vessels cavitate and refill diurnally or are R-shaped curves invalid in *Robinia*? *Plant, Cell & Environment* **37**: 2667–2678.

Wheeler JK, Huggett BA, Tofte AN, Rockwell FE, Holbrook NM. 2013. Cutting xylem under tension or supersaturated with gas can generate PLC and the appearance of rapid recovery from embolism. *Plant, Cell & Environment* **36**: 1938–1949.

Yin P, Cai J. 2018. New possible mechanisms of embolism formation when measuring vulnerability curves by air injection in a pressure sleeve. *Plant, Cell & Environment* **41**: 1361–1368.

Zhang FP, Brodribb TJ. 2017. Are flowers vulnerable to xylem cavitation during drought? *Proceedings of the Royal Society of London. Series B: Biological Sciences* **284**: 20162642.

Zhang Y, Lamarque LJ, Torres-Ruiz JM, Schuldt B, Karimi Z, Li S, Qin DW, Bittencourt P, Burlett R, Cao KF *et al.* 2018. Testing the plant pneumatic method to estimate xylem embolism resistance in stems of temperate trees. *Tree Physiology* **38**: 1016–1025.

Zhang YJ, Holbrook NM. 2014. The stability of xylem water under tension: a long, slow spin proves illuminating. *Plant, Cell & Environment* **37**: 2652–2653.

Zhu SD, Chen YJ, Fu PL, Cao KF. 2017. Different hydraulic traits of woody plants from tropical forests with contrasting soil water availability. *Tree Physiology* **37**: 1469–1477.

Zimmermann MH. 1983. *Xylem structure and the ascent of sap*. Berlin, Germany: Springer.

Supporting Information

Additional Supporting Information may be found online in the Supporting Information section at the end of the article.

Fig. S1 A test to determine how the length of time samples are immersed in the water affects the gas-filled vessels over time when using MicroCT scanning.

Fig. S2 Confidence intervals for differences between the mean P_{50} values for each method.

Fig. S3 Comparison of embolism levels derived using the hydraulic and the MicroCT methods applied to the same stem segments.

Fig. S4 The relationships between xylem structural traits and the discrepancy ratios of P_{50}-PAD and P_{50}-AI against P_{50}-MicroCT.

Fig. S5 The differential vacuum pressure changes over 2.5 min in samples with different sample lengths for three stems of *Microcos paniculate*.

Fig. S6 The differential vacuum pressure changes over 2.5 min in samples with different sample lengths for three stems of *Lasiococca comberi*.

Fig. S7 The differential vacuum pressure changes over 2.5 min in samples with different sample lengths for two stems of *Combretum griffithii*.

Fig. S8 The differential vacuum pressure changes over 2.5 min in samples with different sample lengths for two stems of *Combretum yunnanense*.

Fig. S9 A diagrammatic representation of air sources extracted from a stem and the spread of embolisms with use of the pneumatic-air-discharge method.

Fig. S10 Shrinkage of xylem tissue at different stages of desiccation as recorded in MicroCT images.

Methods S1 Methods for determining the maximum vessel length.

Methods S2 The AI method.

Methods S3 Methods for the tests of sample length and shrinkage effects when using the PAD method.

Table. S1 A literature survey summary of studies conducted since 2010 that have used different methods to construct xylem vulnerability curves.

Please note: Wiley Blackwell are not responsible for the content or functionality of any Supporting Information supplied by the authors. Any queries (other than missing material) should be directed to the *New Phytologist* Central Office.